Hindawi Publishing Corporation
International Journal of Rotating Machinery
Volume 2008, Article ID 536079, 12 pages
doi:10.1155/2008/536079

Research Article

Quasi-Steady Analytical Model Benchmark of an Impulse Turbine for Wave Energy Extraction

A. Thakker, J. Jarvis, and A. Sahed

Department of Mechanical & Aeronautical Engineering, Materials and Surface Science Institute, University of Limerick, Limerick, Ireland

Correspondence should be addressed to A. Sahed, amar.sahed@ul.ie

Received 15 April 2008; Accepted 11 September 2008

Recommended by Ion Paraschivoiu

This work presents a mean line analysis for the prediction of the performance and aerodynamic loss of axial flow impulse turbine wave energy extraction, which can be easily incorporated into the turbine design program. The model is based on the momentum principle and the well-known Euler turbine equation. Predictions of torque, pressure drop, and turbine efficiency showed favorable agreement with experimental results. The variation of the flow incidence and exit angles with the flow coefficient has been reported for the first time in the field of wave energy extraction. Furthermore, an optimum range of upstream guide vanes setting up angle was determined, which optimized the impulse turbine performance prediction under movable guide vanes working condition.

1. INTRODUCTION

The oscillating water column (OWC) wave energy harnessing method is considered as one of the best techniques of converting wave energy into electricity. It is an economically viable design due to its simple geometrical construction, and is also strong enough to withstand against the waves with different heights, periods, and directions. The design (see Figure 1) consists of an OWC chamber and a circular duct, which reciprocally moves the air from and into the chamber as the wave enters and intercedes from the chamber. The wave energy is converted into air pneumatic energy inside the chamber. A special turbine mounted inside the duct converts the air pneumatic energy to a mechanical power. A matching generator is coupled to the turbine to produce electricity [1].

In order to use the potential wave energy resource, efficiently, turbine design/operation with low losses, high efficiency, and desirable performance is needed. The efficiency is a measure of performance and a poorly performing turbine becomes unavailable for power plant. Therefore a sound knowledge of the turbine efficiency limits is necessary for the power take-off design/operation.

The impulse turbine discussed here is one of a class of turbines called self-rectifying turbines, that is, turbines that rotate in the same direction no matter what the direction of the airflow is. Self-rectifying turbines are a response to the need for turbines to extract power from bidirectional airflows that arise in wave power applications such as the OWC. The basic turbine design parameters were based on the optimum design parameters given by Setoguchi and Takao [2], but with a H/T ratio of 0.6. The details are given in Table 1 and a 2D sketch at mid radius is shown in Figure 2. The rotor consists of 30 blades with a chord length, $L_r = 100$ mm and pitch, $S_r = 50$ mm. There are 26 fixed angle mirror image guide vanes on both sides of the rotor. The guide vanes inlet/outlet angle is fixed at 30°. The turbine was tested at a constant axial air velocity of 7.22 m/s. Data were collected with the help of data acquisition system to minimize the errors. Experiments were performed by varying the rotational speed from 1300 to 100 rpm, thus giving a flow coefficient range of 0.22–2.90 under unidirectional steady flow conditions. The peak efficiency of 44.6% was achieved at $\phi = 0.88$, corresponding to a rotational speed of 300 rpm. The Reynolds number at the peak efficiency point was 0.92×10^5.

The state-of-the-art of the wave energy impulse turbine is crucially getting closer to an actual prototype and an analytical model of the turbine derived from first principles would prove necessary. Thus far, the highest efficiency reported by model testing has been 50% at most, which

Table 1: Rotor and guide vanes geometry.

Parameter	Symbol	$H/T = 0.6$
Blade profile: elliptical		
Number of blades	z	30
Tip diameter	D	600.0 mm
Chord length	L_r	100.0 mm
Blade passage flow	T_a	20.04 mm
Pitch	S_r	50 mm
Blade inlet angle	γ	60°
Guide vanes profile: plate type		
Pitch	S_g	58.0 mm
Chord length	L_g	131.0 mm
Number of guide vanes	g	26
Guide vane inlet/outlet angle		30°

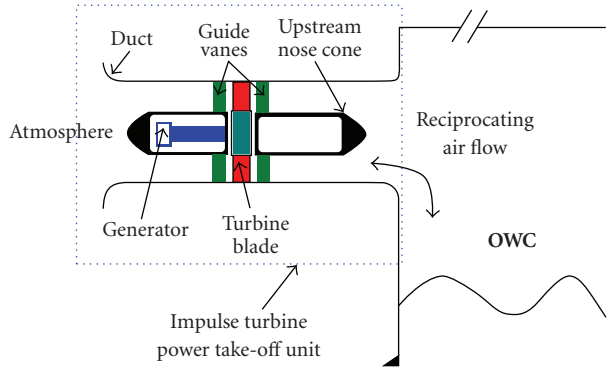

Figure 1: Impulse turbine power take-off unit with OWC.

makes this particular impulse turbine underperforming the conventional axial turbine by a wide margin. Partly, this is due to the fact that designing a turbine for a wave power application requires that a design range be taken into account, rather than a single design point [3]. Furthermore, the operational environment to which the turbine must be designed is inherently random, constantly varying, and difficult to predict. Therefore, the prediction of operational flow coefficients is potentially problematic. The flow when passes through rotor stagnation and static properties changes. If there is no static pressure drop in a rotor, the turbine is called impulse turbine. Experimental studies showed that in this turbine, though typified under "Impulse," a substantial degree of reaction is present [4], which tells about the amount of losses generated in the turbine blade passage.

Using simple performance prediction of the flow at the mean line of blade height combined with numerical method, an explicitly new analytical model for estimating the maximum efficiency of wave energy extraction impulse turbine of any size is presented and compared favorably to a set of experimental data. The theoretical analysis which, based on the angular momentum principle and Euler turbine equation, yields the turbine performance parameters previously obtained by model testing under quasi-steady

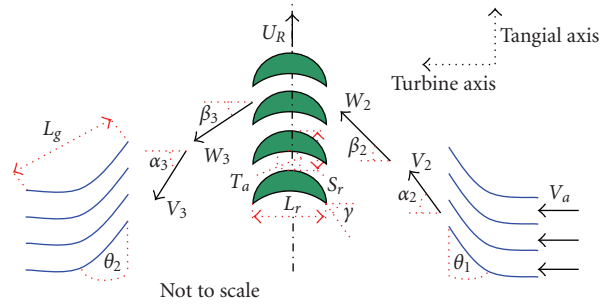

Figure 2: Impulse turbine geometry and velocity vectors.

state. The model yields equations that predict the shape of the curves obtained by plotting the experimental data.

2. TURBINE WORKING PRINCIPLE

The working principle of the impulse turbine should be well understood in order to optimize the design of the power take-off unit. In order to achieve this, velocity triangles can be used to calculate the basic performance of the turbine. Figure 2 shows the relevant velocities along with the turbine blades and guide vane geometry.

The air issued from the OWC is constrained to exit to the atmosphere through the turbine duct. In the annular duct, the air flows axially with a velocity V_a before it gets diverted with an angle α_2 with respect to the turbine axis by the inlet guide vanes located upstream of the turbine rotor. Besides the introduction of the prewhirl angle α_2, the inlet guide vanes play a role of stationary nozzles for which the purpose is to accelerate and guide the flow smoothly into the rotor. The air exits the upstream guide vanes at absolute velocity V_2 which is higher than V_a. A certain amount of static pressure drop is achieved through the nozzle. Therefore, the air flow gains in dynamic pressure and looses in static pressure when passing the inlet guide vanes. The rotor rotates at velocity U_R and relative to the rotor, the velocity of the air as it impinges on the rotor entrance is W_2. The air is turned by the rotor and exits, relative to the rotor, at velocity W_3. However, in absolute terms the rotor exit velocity is V_3.

2.1. Turbine losses

Flows through an axial turbine blade passage are always three-dimensional, viscous, and unsteady. Both the geometric description of the fluid flow domain and the physical processes present are extremely complicated [5]. Nevertheless, the flow through the wave energy impulse turbine is considered incompressible with subsonic regime as the flow rates generated by the OWC are relatively low. But regions of laminar, transitional, and turbulent flows, separated flows, and fully developed viscous profiles may all be present simultaneously due to the complicated geometry of the flow field.

In general the losses generated within the turbine passage consists of profile loss, secondary flow loss, tip clearance loss, and mechanical loss. The latter could be reduced with

improved manufacturing and assembling technology, and profile and secondary flow loss (60%) could be reduced by designing a turbine to operate at optimum design parameters. However, there are many design parameters for minimizing aerodynamic losses within the turbine passage. Among them, the incidence angle is the most important as it is immediately related to the aerodynamic losses [6]. The guide vanes and blade profile losses can be significant if the blade shapes are not optimized for the local operating conditions. Profile losses are driven by surface finish, total blade surface area, blade shape and surface velocity distributions, and proper matching between guide vane and blade to minimize incidence losses. Equally significant losses can be caused by the complex secondary flows generated as the viscous boundary layers along the pressure and suction of the air path are turned through the blade passage.

The clearance between the blade tips and casing endwall in a turbine induces leakage flow, which arises due to pressure difference between the pressure surface and suction surface of the blade. The leakage flow emerging from the clearance interacts with the passage flow (main stream) and rolls up into a vortex known as tip leakage vortex. Although the size of the clearance is typically about 1% of the blade height, the leakage flow through this small clearance has a significant effect on the aerodynamics of the turbine. For example, the tip clearance loss of a turbine blade can account for as much as one-third of the total losses [7]. The tip leakage loss is driven by the higher reaction levels at the blade tip, which increases the pressure drop across the blade tip.

In contrast to the general design problem familiar in industry (e.g., steam and gas turbines), where a turbine would be expected to operate at a single design point for the majority of the time, the performance of a turbine intended for use in a wave energy application must be considered over a range of flow coefficient. This is a consequence of the constantly changing and bidirectional nature of the airflow (varying loads), thus designing a turbine to a wave power application requires that a design range be taken into account, rather than a single design point [3]. Nevertheless, a certain similarity can be found between the steam impulse turbine and the self-rectifying impulse turbine as for both the fluid's pressure is changed to velocity by accelerating the fluid with a nozzle and upstream guide vane, respectively. Also, the steam rotor blade can be recognized by its shape, which is symmetrical about the rotor midchord and has inlet and exit angles around 20°. It has constant cross section from hub to tip, which is almost similar to that of the wave energy impulse turbine.

2.2. Flow incidence and deviation angle

The relative inlet flow vector at blade leading edge (W_2) is not a simple geometric value but a measured parameter; that is, it depends on the rotational speed and the absolute flow velocity. The incidence i on the rotor is defined as an angle calculated from the relative inlet flow vector to the blade inlet angle (see Figure 3). Optimizing the incidence would minimize pressure losses in the blade passage, which the turbine efficiency is directly related to. The optimum

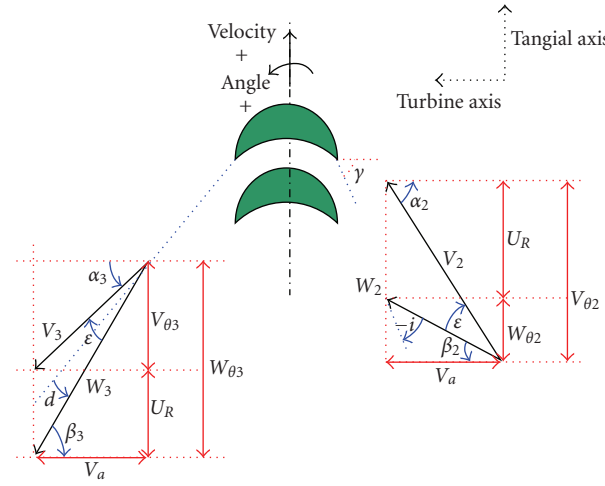

Figure 3: Velocity triangles.

incidence depends on the input power as well as the blade profile. The range of applicable incidence becomes narrow when the turbine operates at high input power [8]. Also, due to Cho and Choi [8] the optimum is for small negative values (around −20°) but the efficiency quickly drops as the incidence grows to negative over the range of applicable incidence, in which case the flow tends to strike the blade leading edge axially and beyond.

The angle of the flow leaving the blade at the trailing edge (β_3) is of great importance as it determines the magnitude of relative exit flow at blade trailing edge (W_3). The deviation angle (d) from the rotor is defined as an angle calculated from the relative exit flow vector to the blade exit angle. Assuming that the axial velocity and the relative tangential velocity remain the same (for optimum design flow coefficient), the angle β_3 is dependant on the geometry profile of the blade's trailing edge and the pressure difference between the suction side and pressure side [4, 9].

The basic objective of the turbine design is that the blade angles at inlet and exit γ must be matched properly with the fluid flow angles (β_2, β_3), respectively. They need not necessarily be equal, but should be matched properly to minimize losses [4].

The absolute angle (α_3) at the blade trailing edge is equally important as it determines the absolute velocity (V_3) by which the air flow enters the inlet of the downstream guide vanes. If the angle α_3 is close to 60°, the metal blade angle, then the air would enter the downstream guide vanes swiftly as the air flow direction would be parallel to the straight portion of the guide vanes. Under this condition, the wave energy impulse turbine would be working at maximum efficiency because of the reduced losses through the downstream guide vanes [4, 9]. These losses are known, from experimental work, to be substantial and directly affect the turbine efficiency. Outside the above working condition, the air will strike the guide vanes more or less axially, causing bigger losses. In the latter case, the turbine is said to be off-designed. For an ideal wave energy impulse turbine, α_3 should also match the setting up angle of the downstream

guide vanes, θ_2, which adds to the complexity of the design (see Figure 2).

2.3. Turbine performance evaluation

Thus far the turbine characteristics under steady flow conditions have been obtained by model testing and were evaluated according to the torque coefficient C_t, input power coefficient C_a and flow coefficient ϕ, which are defined by Setoguchi and Takao [2]:

$$C_t = \frac{T_o}{(1/2)\rho_a(V_a{}^2 + U_R{}^2)bZL_r r_R}, \quad (1)$$

$$C_a = \frac{\Delta PQ}{(1/2)\rho_a(V_a{}^2 + U_R{}^2)bZL_r V_a}, \quad (2)$$

$$\phi = \frac{V_a}{U_R}, \quad (3)$$

$$R_e = \frac{\rho_a\sqrt{V_a{}^2 + U_R{}^2}L_r}{\mu}, \quad (4)$$

$$\eta = \frac{C_t}{C_a\phi}, \quad (5)$$

where R_e is the Reynolds number based on the chord length, T_o: measured output torque, ρ_a: density of air, b: rotor blade height, U_R: circumferential at r_R, V_a: mean axial flow velocity, r_R: mean radius, Z number of rotor blades, ΔP: measured total pressure drop between settling chamber and atmosphere, and Q: flow rate. The test Reynolds number based on the chord was 0.4×10^4.

On the other hand, it was reported in [10] that the quasi-steady torque and input coefficient were higher, especially at high flow coefficient than those found when the turbine is operated under unsteady flow conditions. Also, the drop-off in efficiency under steady state at high flow coefficient was not seen under sinusoidal flow pattern. Furthermore, the sinusoidal testing showed that if the efficiency is considered through the complete sinusoidal wave, it is relatively constant. Therein, it is therefore important that future turbines are designed with this in mind due to the difference between the results found from unsteady testing and those predicted using fixed flow testing.

Velocity triangles can be constructed at any section through the blades (e.g., hub, tip, midsection, etc.) using the various velocity vectors, but are usually shown at the mean radius. The obvious snag is that of the reduction in aerodynamic design work. At other radii velocity triangles will vary, demanding the introduction of either blade or guide vanes twisting [11]. Nevertheless, it is known that the efficiency of a properly designed axial flow turbine can be predicted with fair accuracy (1 or 2%) by the adoption of simple mean line analysis methods which incorporate proper loss and flow angle correlations [12].

Similar to simple theory for ordinary turbo-machine, the following assumption can be given to analyze the turbine performance.

(i) Turbine performance is estimated from condition at mean radius.

(ii) Absolute nozzle exit flow angle α_2, the complement of θ_1, is constant.

(iii) Relative rotor exit flow angle is constant, β_3.

Due to blade symmetry of this particular design of self rectifying turbine we can state that

(iv) the angles between the relative flow vector and the absolute velocity vector at inlet and outlet of the rotor are identical (ϵ).

3. TORQUE ANALYSIS

Applying "momentum principle—Newton's second law," the torque generated by the turbine shaft due to the tangential momentum change of air passing through the turbine rotor can be evaluated as follows [11]:

Generated torque = rate of change of moment of momentum:

$$T_o = \frac{d}{dt}(mr_R\Delta V). \quad (6)$$

Replacing the expression of change of air whirl velocity in (6), we get

$$T_o = \dot{m}r_R U_R\left(\frac{V_{\theta 2}}{U_R} + \frac{V_{\theta 3}}{U_R}\right). \quad (7)$$

From the velocity diagram of Figure 3, we have

$$\frac{V_{\theta 2}}{U_R} = \phi\left(\frac{W_{\theta 2} + U_R}{V_a}\right) = \phi\tan\beta_2 + 1,$$
$$\frac{V_{\theta 3}}{U_R} = \phi\tan\alpha_3. \quad (8)$$

Replacing (8) in (7), the torque is expressed as

$$T_o = \dot{m}r_R U_R\phi\left(\tan\beta_2 + \tan\alpha_3 + \frac{1}{\phi}\right). \quad (9)$$

By the replacement for the expression of $\dot{m}$ and using blade height, chord length, and flow coefficient definition, we get from (9)

$$T_o = \frac{1}{2}\rho U_R{}^2 bZL_r r_R 2\left(\frac{\pi D_r}{ZL_r}\right)\phi^2\left(\tan\beta_2 + \tan\alpha_3 + \frac{1}{\phi}\right). \quad (10)$$

Multiplying and dividing (10) through $(1 + \phi^2)$, we get

$$T_o = \left\{\frac{1}{2}\rho U_R{}^2(1+\phi^2)bZL_r r_R\right\}2\left(\frac{\pi D_r}{ZL_r}\right)\left(\frac{\phi^2}{1+\phi^2}\right) \times\left(\tan\beta_2\tan\alpha_3 + \frac{1}{\phi}\right). \quad (11)$$

Now, we define the theoretical torque coefficient $(C_t)_{\mathrm{Th}}$ as

$$(C_t)_{\mathrm{Th}} = \frac{T_o}{\{(1/2)\rho U_R{}^2(1+\phi^2)bZL_r r_R\}}, \quad (12)$$

$$(C_t)_{\mathrm{Th}} = 2\left(\frac{\pi D_r}{ZL_r}\right)\left(\frac{\phi^2}{1+\phi^2}\right)\left(\tan\beta_2 + \tan\alpha_3 + \frac{1}{\phi}\right). \quad (13)$$

The term contained in the first brackets of (13) is the inverse of the turbine rotor solidity σ_r;

$$(C_t)_{\text{Th}} = \frac{2}{\sigma_r}\left(\frac{\phi^2}{1+\phi^2}\right)\left(\tan\beta_2 + \tan\alpha_3 + \frac{1}{\phi}\right). \tag{14}$$

From (8) we have

$$\begin{aligned} \Longrightarrow \tan\alpha_2 &= \tan\beta_2 + \frac{1}{\phi}, \\ \beta_2 &= \arctan\left(\tan\alpha_2 - \frac{1}{\phi}\right). \end{aligned} \tag{15}$$

Defining the incidence on the rotor i, as an angle calculated from the relative inlet flow vector W_2 to the blade angle α_2;

$$i = \beta_2 - \gamma = \arctan\left(\tan\alpha_2 - \frac{1}{\phi}\right) - \gamma. \tag{16}$$

The incidence is negative as shown in Figure 3.

The angle β_3 is dependant on the geometry profile of the blade's trailing edge and the pressure difference between the suction side and pressure side. Hill and Peterson (1992, 1994) [12] reported that β_3 can be evaluated as

$$\beta_3 = \arccos\left(\frac{Ta}{Sr}\right). \tag{17}$$

From which we can evaluate the deviation angle d as

$$d = \beta_3 - \gamma. \tag{18}$$

The deviation angle is positive as shown in Figure 3.

From assumption 3 and velocity diagram Figure 3,

$$\alpha_3 = \beta_3 - \epsilon = \arccos\left(\frac{Ta}{Sr}\right) - \epsilon. \tag{19}$$

4. PRESSURE DROP ANALYSIS

From Figure 3, we have

$$V_{\theta 3} = W_{\theta 3} - U_R. \tag{20}$$

Using (7), we get the output power as

$$\begin{aligned} P_o &= T_o\omega = \dot{m}U_R(V_{\theta 2} + W_{\theta 3} - U_R), \\ \frac{dP_o}{dU_R} &= \dot{m}(V_{\theta 2} + W_{\theta 3} - 2U_R) = 0. \end{aligned} \tag{21}$$

Therefore when

$$\begin{aligned} U_R &= \frac{V_{\theta 2} + W_{\theta 3}}{2} \\ \Longrightarrow P_o &= P_{o,\max} = \frac{\rho}{4}(V_{\theta 2} + W_{\theta 3})^2 Q. \end{aligned} \tag{22}$$

Given that the maximum power output equals the available power to the turbine rotor at blade inlet

$$\Longrightarrow P_{o,\max} = \Delta P_{\text{th}} Q, \tag{23}$$

where ΔP_{th} is the pressure gradient across the turbine rotor, which can be estimated as

$$\Delta P_{\text{th}} = \frac{\rho}{4}(V_{\theta 2} + W_{\theta 3})^2. \tag{24}$$

On the other hand,

$$\Delta PQ = \dot{m}I, \tag{25}$$

where ΔP is the actual pressure gradient across the turbine (including the guide vanes) and I is the actual enthalpy drop through the turbine. The latter equals the theoretical enthalpy drop of the turbine (I_{th}) plus enthalpy loss through the turbine (ΔI_1) which in turn is related to the total loss coefficient ζ by [13]

$$\zeta = \frac{\Delta I_1}{(1/2){V_a}^2}. \tag{26}$$

Using (25) and the definition of the actual enthalpy ($I = I_{\text{th}} + \Delta I_1$), we get

$$\begin{aligned} \Longrightarrow \Delta P &= \frac{\dot{m}}{Q}I_{\text{th}} + \frac{\dot{m}}{Q}\Delta I_1 \\ &= \Delta P_{\text{th}} + \Delta P_L, \end{aligned} \tag{27}$$

where ΔP_L is a measure of pressure losses through the turbine (including the guide vanes and tip clearance losses):

$$\Delta P_L = \frac{1}{2}\zeta\rho{V_a}^2, \tag{28}$$

$$\Delta P = \frac{1}{2}\rho\frac{(V_{\theta 2} + W_{\theta 3})^2}{2} + \frac{1}{2}\zeta\rho{V_a}^2. \tag{29}$$

Multiplying both sides of (29) by Q, we get the input power as

$$\Delta PQ = \frac{1}{2}\rho{V_a}^2\left\{\frac{1}{2}\left(\frac{V_{\theta 2}}{V_a} + \frac{W_{\theta 3}}{V_a}\right)^2 + \zeta\right\} bZL_r\left(\frac{\pi D_r}{ZL_r}\right)V_a. \tag{30}$$

Multiplying and dividing through $(1+\phi^2)$, (30) becomes

$$\begin{aligned} \Delta P\,Q = &\left\{\frac{1}{2}\rho{U_R}^2(1+\phi^2)bZL_rV_a\right\}\left(\frac{\pi D_r}{ZL_r}\right)\left(\frac{\phi^2}{1+\phi^2}\right) \\ &\times\left\{\frac{1}{2}\left(\tan\beta_2 + \tan\alpha_3 + \frac{2}{\phi}\right)^2 + \zeta\right\}. \end{aligned} \tag{31}$$

Now, we define the theoretical input coefficient $(C_a)_{\text{Th}}$ as

$$\begin{aligned} (C_a)_{\text{Th}} &= \frac{\Delta PQ}{\{(1/2)\rho{U_R}^2(1+\phi^2)bZL_rV_a\}}, \\ (C_a)_{\text{Th}} &= \frac{1}{\sigma_r}\left(\frac{\phi^2}{1+\phi^2}\right)\left\{\frac{1}{2}\left(\tan\beta_2 + \tan\alpha_3 + \frac{2}{\phi}\right)^2 + \zeta\right\}. \end{aligned} \tag{32}$$

4.1. Loss coefficient ζ

Losses in turbines are used to be expressed in terms of loss coefficients. They are manifested by a decrease in stagnation enthalpy, and a variation in static pressure, compared to the isentropic flow. The commonly used loss coefficient is the stagnation pressure loss coefficient, which is convenient for experimental work and especially for this particular impulse turbine. Wei [14] has reported in his doctoral thesis by referring back to Horlock [15] that the incidence is the most important parameter to predict the off-design profile loss. The stagnation pressure loss coefficient in the relative frame is defined as [16]

$$\zeta_R = \frac{P_{02,\mathrm{rel}} - P_{03,\mathrm{rel}}}{(1/2)\rho {W_2}^2}, \tag{33}$$

where $P_{0,\mathrm{rel}} = P + (1/2)\rho W^2$ is the relative total pressure at blade inlet and outlet (2, 3), respectively.

From (33) we have

$$\zeta_R = \frac{(P_2 + (1/2)\rho {W_2}^2) - (P_3 + (1/2)\rho {W_3}^2)}{(1/2)\rho {W_2}^2}, \tag{34}$$

$$\zeta_R = \frac{(P_2 + (1/2)\rho {W_2}^2) - (P_3 + (1/2)\rho {W_3}^2)}{(1/2)\rho {W_2}^2} + \frac{(1/2)\rho({V_2}^2 - {V_2}^2) + (1/2)\rho({V_3}^2 - {V_3}^2)}{(1/2)\rho {W_2}^2}, \tag{35}$$

$$\zeta_R = \frac{(P_2 + (1/2)\rho {V_2}^2) - (P_3 + (1/2)\rho {V_3}^2)}{(1/2)\rho {W_2}^2} + \frac{({W_2}^2 - {V_2}^2) + ({V_3}^2 - {W_3}^2)}{{W_2}^2}. \tag{36}$$

Multiplying and dividing through ${V_2}^2$ (36), rearranging we get

$$\zeta_R = \left(\frac{V_2}{W_2}\right)^2 \left\{ \underbrace{\frac{(P_2 + (1/2)\rho {V_2}^2) - (P_3 + (1/2)\rho {V_3}^2)}{(1/2)\rho {V_2}^2}}_{A} + \underbrace{\left(\frac{W_2}{V_2}\right)^2 - 1 + \left(\frac{V_3}{V_2}\right)^2 - \left(\frac{W_3}{V_2}\right)^2}_{B} \right\}. \tag{37}$$

Applying Euler turbine equation [10],

$$\left(P_2 + \frac{1}{2}\rho {V_2}^2\right) - \left(P_3 + \frac{1}{2}\rho {V_3}^2\right) = \rho U_R (V_{\theta 2} + V_{\theta 3}) \tag{38}$$

$$\Longrightarrow A = \frac{\rho U_R (V_{\theta 2} + V_{\theta 3})}{(1/2)\rho {V_2}^2} \tag{39}$$

$$A = 2\left(\frac{U_R}{V_2}\right)^2 \left(\frac{V_a}{U_R}\right)\left(\frac{V_{\theta 2}}{V_a} + \frac{V_{\theta 3}}{V_a}\right). \tag{40}$$

From Figure 3 we have $V_2 = V_a/\cos\alpha 2$, $\tan\alpha 2 = V_{\theta 2}/V_a$, and $\tan\alpha_3 = V_{\theta 3}/V_a$

$$\Longrightarrow A = \frac{2}{\phi}(\cos\alpha_2)^2(\tan\alpha_2 + \tan\alpha_3). \tag{41}$$

Also, from Figure 3 we have $W_2 = V_a/\cos\beta_2$, $W_3 = V_a/\cos\beta_3$, and $V_3 = V_a/\cos\alpha_3$

$$\Longrightarrow B = (\cos\alpha_2)^2 \left\{ \frac{1}{(\cos\beta_2)^2} - \frac{1}{(\cos\alpha_2)^2} + \frac{1}{(\cos\alpha_3)^2} - \frac{1}{(\cos\beta_3)^2} \right\}. \tag{42}$$

By replacing (39) and (42) in (37), simplifying, and rearranging, we get

$$\zeta_R = (\cos\beta_2)^2 \left\{ \frac{2(\tan\alpha_2 + \tan\alpha_3)}{\phi} + \frac{1}{(\cos\beta_2)^2} - \frac{1}{(\cos\alpha_2)^2} + \frac{1}{(\cos\alpha_3)^2} - \frac{1}{(\cos\beta_3)^2} \right\}, \tag{43}$$

ζ_R accounts only for aerodynamic losses (profile and secondary flow losses, which cannot be separated) through the blade passage. These are greatly affected by the flow incidence [7, 11]. Therefore the tip clearance loss and the loss in the turbine stationary guide vanes are not accounted for. For this, an underestimation of the actual losses is to be expected when only using the losses in the rotor (43). The actual losses would be accurately simulated if we could have an expression of ζ which accounts for all the losses in the turbine (including tip clearance leakage, guide vanes, near hub, and casing walls losses). For the particular WERT test rig, UL, the data logger acquisition compensates the torque measurement for the mechanical and windage losses.

It was reported from model testing that substantial stagnation pressure drop across the downstream guide vane exists causing losses. To take these into account, estimation from three-dimensional computational fluid dynamics (CFD) of the losses across the downstream guide vanes was utilized.

The variation of pressure loss coefficient through the downstream guide vane at various stations from hub to tip was computed for the flow coefficients $\phi = 0.45, 0.67, 1, 1.35$, and 1.68, respectively. The total pressure loss coefficient has been defined as follows [17–19]:

$$\zeta_{\mathrm{GV}} = \frac{P_{oi} - P_o}{P_{oi} - P_{si}}, \tag{44}$$

where P is the pressure and the subscripts i, o, and s denote inlet conditions, total and static conditions, respectively.

Then, the arithmetic mean of the computed values from hub to tip for each flow coefficient were calculated, plotted and an optimum curve fit correlation ($\zeta_{\mathrm{GV}} = f(\phi)$) was established as illustrated in Figure 4;

$$\zeta_{\mathrm{GV}} = \frac{5.78}{\phi} - 1.85. \tag{45}$$

The correlation of the downstream guide vane loss (45) derived from validated computational (CFD) work should be

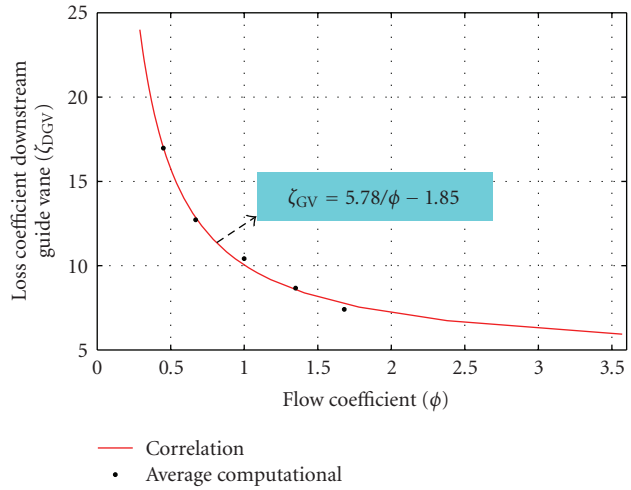

Figure 4: Correlated downstream guide vane loss coefficient versus flow coefficient [10].

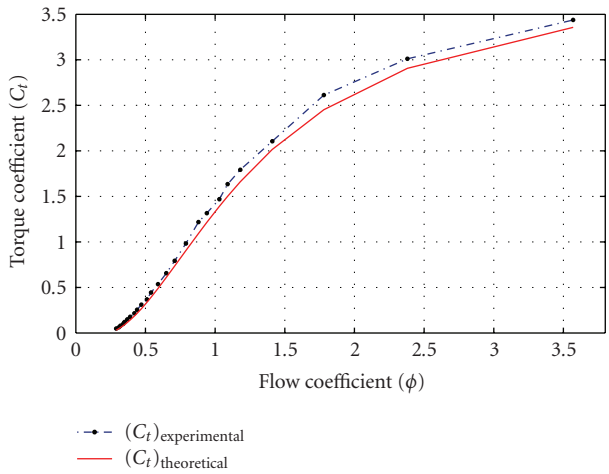

Figure 5: Turbine torque coefficient versus flow coefficient [10].

considered specific for the design of impulse turbine wave energy extraction;

$$\zeta = \zeta_R + \zeta_{GV}. \tag{46}$$

5. RESULTS AND DISCUSSION

Figure 5 shows the theoretical and experimental torque coefficient versus flow coefficient. The torque coefficient follows an exponential trend up to flow coefficient ($\phi = 0.8$) then a short transition occurs and the trend becomes logarithmic in nature for the rest of the flow coefficient. There is no apparent stall, as opposed to the Wells turbine. It can be seen that the model's torque coefficient predicts well the shape of the torque coefficient obtained by plotting the experimental data. The prediction seems to be almost perfect at low flow coefficient (up to $\phi = 0.8$) and then a small discrepancy appears for the rest of the flow coefficient.

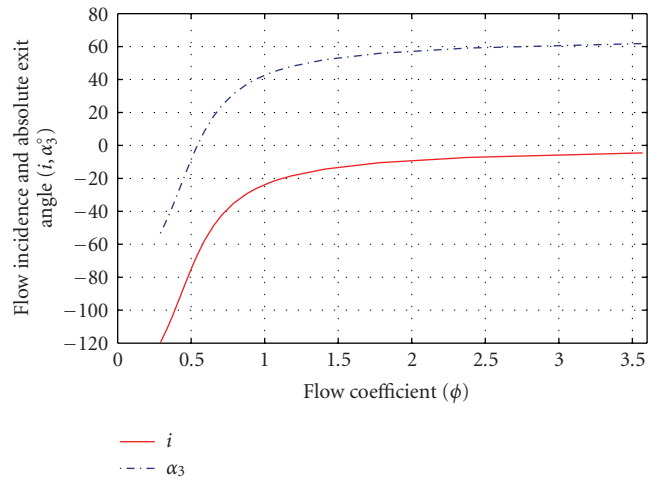

Figure 6: Flow incidence and absolute exit angle versus flow coefficient.

Figure 6 shows the variation of the incidence angle (i) and absolute exit angle (α_3), calculated from (16) and (19), respectively, with the flow coefficient. The incidence angle, directly related to the profile geometry [9], is very high (negative) at low flow coefficients (high rotational speed) making the air flow relatively impinging at the suction side of the leading edge. In other word, the stagnation point is located at the suction side of the leading edge and the air flow acts as a break on the turbine. This would be the main reason of the negative torque obtained experimentally [4]. As the flow coefficient increases a rapid decline of the incidence occurs from -120° at $\phi = 0.29$ up to $\phi = 1.1$ at which it reaches -20°, where the turbine efficiency reaches a plateau. The optimum incidence angle for wave energy impulse turbine is for small negative values (around -20°) similar to that reported in [5]. At this condition the stagnation point is located close on the end profile camber line. As the flow coefficient continues increasing the incidence angle is decreasing almost steadily to reach a value of -4.5° at the highest flow coefficient of $\phi = 3.57$. At this low incidence angle the relative flow angle (β_2, (16)) is almost aligned with the blade angle (γ) presenting a supposedly optimum working conditions, where the incidence angle ensures the smoothest entry condition into the turbine rotor blade.

The trend of the exit angle is similar, but varies in phase (66°) with the incidence angle, Figure 6. At very low flow coefficient $\phi = 0.29$, the absolute exit flow angle is about -55° causing the flow to impinge onto the downstream guide vane straight portion vertically (the ideal is when the flow direction is parallel to the downstream guide vane straight portion, smooth entry). Then, a rapid decrease (from high negative value) of the exit flow angle is shown with the increase of flow coefficient, reaching 46° at $\phi = 1.1$. At this flow coefficient the flow entering the inlet guide vane is relatively smooth. In between the above two flow coefficients, there was a condition where the exit flow vector V_3 became aligned with the axial flow vector V_a, precisely at a value of flow coefficient $\phi = 0.53$. As the flow coefficient continues

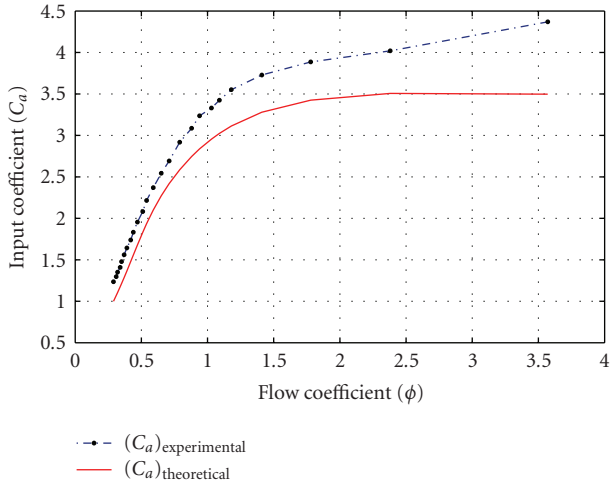

Figure 7: Turbine input coefficient versus flow coefficient [10].

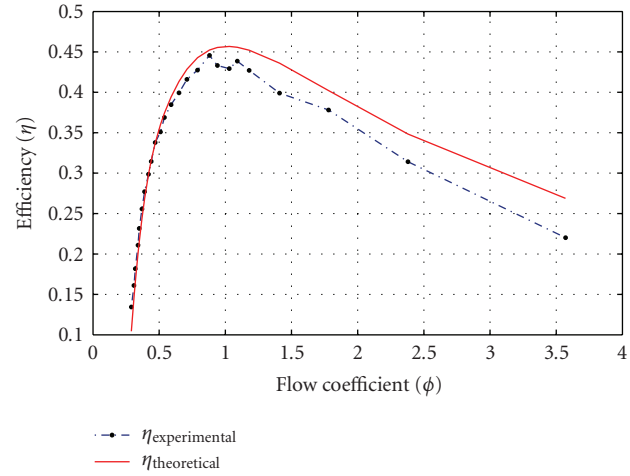

Figure 8: Turbine efficiency versus flow coefficient [10].

beyond $\phi = 1.1$, a steady increase of exit flow angle is shown up to the highest flow coefficient of $\phi = 3.57$ at which it reaches 62.8°. During the steady increase of the absolute exit flow angle, a favorable working condition sets up, where the exit flow vector becomes closer to the alignment with the downstream guide vane. This will reduce greatly the losses through downstream guide vanes as will be shown below.

Figure 7 displays the input coefficient theoretical and experimental data versus flow coefficient in the case of the losses through the rotor passage and the downstream guide vanes were taken into account (based on experimental analysis the upstream guide vane losses were found to be low [4, 9]). It can be seen that the discrepancy is smaller relative to the earlier case especially at low flow coefficient. Also the slope of the model input coefficient at high flow coefficient is almost zero (no change). Whereas at high flow coefficient, the experimental input coefficient seems to increase with the flow coefficient. This could be explained by the boundary layer separation losses at the blade suction side caused by the high inlet relative flow angle (low incidence angle) and higher loading. Also the contention for the front part of the blade tip could be blocked by the inlet boundary layer "aerodynamically closed" and therefore could be sustaining the horseshoe vortex system [18]. Moreover the tip leakage vortex, which is not incorporated in the model, increases separation. Previous author's results [19] obtained from CFD and validated experimentally showed up to 4% of losses could be generated by the gap existing between the blade tip and the duct inner surface for the specific impulse turbine wave energy extraction.

Figure 8 shows the turbine efficiency from the experimental as well as theoretical data, which is typical of the impulse turbine used for wave energy conversion [2]. At low levels of flow coefficient it can be seen that the efficiency is very sensitive to changes in the flow coefficient. Furthermore, the experimental efficiency was maximum ($\eta = 44.6\%$) at flow coefficient ($\phi = 0.88$) which is known as the optimum flow coefficient and the Reynolds number was ($\text{Re} = 0.92 \times 10^5$). Subsequently, the efficiency decreases as the flow coefficient is further increased, although its sensitivity to changes in flow coefficient diminishes. Low flow coefficient thus greatly reduces the efficiency to an extent that the high flow coefficient does not. This is due to the incidence angle which is very high (negative) at low flow coefficients, making the air flow relatively impinging at the suction side of the leading edge. This is shown experimentally as a small positive value or even negative torque in the region of very low coefficient. Also the low flow coefficient region is characterized with instable working conditions where the efficiency could drop or rise sharply for a small turbine angular velocity increase or decrease, respectively. Nevertheless, as the flow coefficient starts increasing from minimum the turbine picks up in performance sharply to reach the optimum. The reason is that the boundary layers are of type turbulent, due to higher Reynolds number in which case the flow separation does not exist. Also at low flow coefficient the turbine inertia is high helping the turbine to reach the optimum performance quickly. The conjugation of these two effects overcomes the very high flow incidence angle effect.

At high flow coefficient though the incidence angle is optimum because of the low turbine rotational speed, still we notice a slight drop in the turbine performance. This can be explained by the effect of boundary layers of type laminar, due to lower Reynolds number, which are prone to separation especially in the tip region [14]. In the boundary layer regions, the velocity deficit and the total pressure loss increase as the Reynolds number decreases (high flow coefficient). Also, here the inertia is not helping to recover the turbine performance as it is low because of the low rotational speed. At moderate flow coefficient the turbine performance is at maximum and the working condition is stable, that is, there is no sudden change in turbine characteristics within this region of flow coefficient. However, the incidence angle and the boundary layers are not favorable in this moderate flow conditions. This high turbine efficiency working region can be characterized as the compromising region, between the incidence

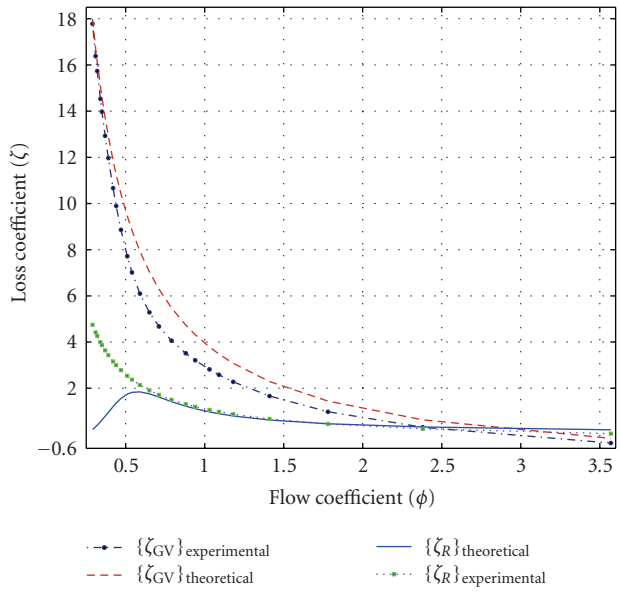

Figure 9: Turbine loss coefficient versus flow coefficient [10].

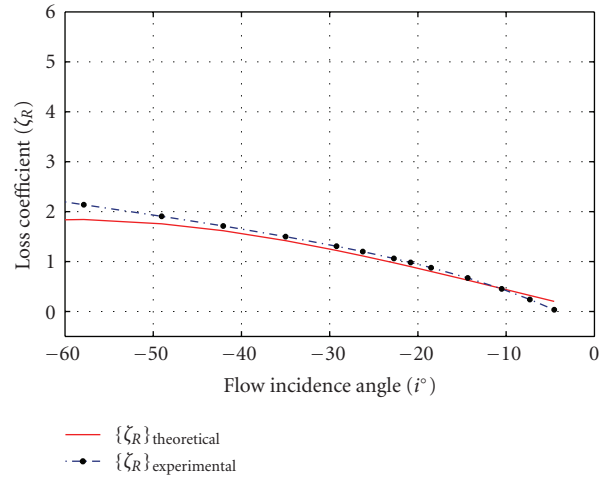

Figure 10: Rotor loss coefficient versus incidence angle [10].

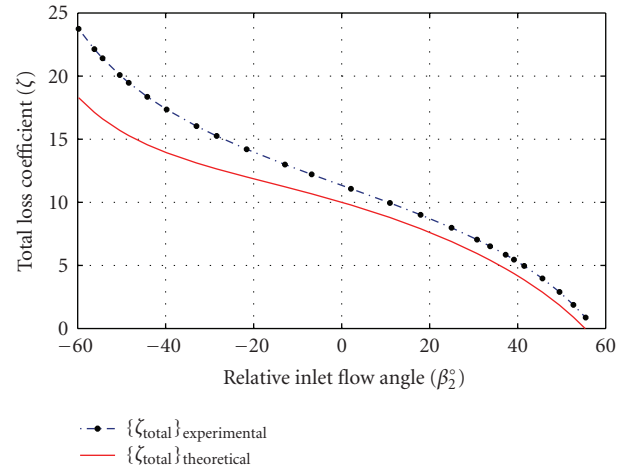

Figure 11: Turbine loss coefficient versus inlet flow angle (β_2) [10].

angle getting closer to the optimum and the boundary layer approaching the turbulent state. Furthermore, this region is characterized as stable due to the impulse turbine reaching the maximum efficiency at low level of torque coefficient.

The model efficiency predicts the experimental data with fair accuracy (2%) overall, though the input coefficient, which does not take into account the tip clearance losses, underpredicts the experimental input coefficient by an average error of (4%). The reason is that the torque coefficient is also underpredicted by the model with an average error of (2%) as can be seen in Figure 5, therefore the ratio of torque coefficient (C_t) and the input coefficient (C_a), which is proportional to the efficiency (5), is lower than it would be if the torque was perfectly predicted.

Figure 9 shows the variation of the experimental and theoretical losses in the blade passage and the downstream guide vane with the flow coefficient. As can be seen the losses through the guide vane decrease rapidly with the increase of the flow coefficient. The model guide vane losses predict well the experimental data at low flow coefficient and a discrepancy appears gradually as the flow coefficient increases. Similar trend can be seen for the experimental losses through the blade passage up to the flow coefficient of ($\phi = 1.1$) and subsequently follows a straight line with a small slope for the rest of the flow coefficient. Whereas the model losses through the blade passage generally decreases following a straight line with a small slope up to the flow coefficient of ($\phi = 1.1$) and then remains almost constant for the rest of the flow coefficient. Particularly, the model predicted loses better through the rotor at high flow coefficient than in the low flow coefficient range. Also, we notice that the level of losses through the guide vane outweighs those of the blade from very low flow coefficient up to ($\phi = 2.7$) at which point the two curves cross each other. Beyond this point, the losses through the guide vanes continue decreasing below zero at high flow coefficient. The small negative value of the losses has been interpreted from model testing of the impulse turbine as a static pressure recovery at outlet downstream guide vanes [4, 18]. Therefore, the behavior of the downstream guide vane in the range of high flow coefficient is similar to that of the diffuser.

Figure 10 depicts the variation of the rotor losses versus the incidence angle. It can be seen from the figure that the losses through the blade passage generally decrease uniformly as the incidence angle decreases from high negative value. In other words, the loss through the rotor is minimized when the incidence angle approaches zero, for which the inlet-flow path is online with the blade angle (see Figure 3).

Figure 11 shows the variation of the experimental and theoretical total losses in the turbine with inlet angle. As can be seen the predicted total losses trend is similar to the experimental data. The level of losses decreases with the

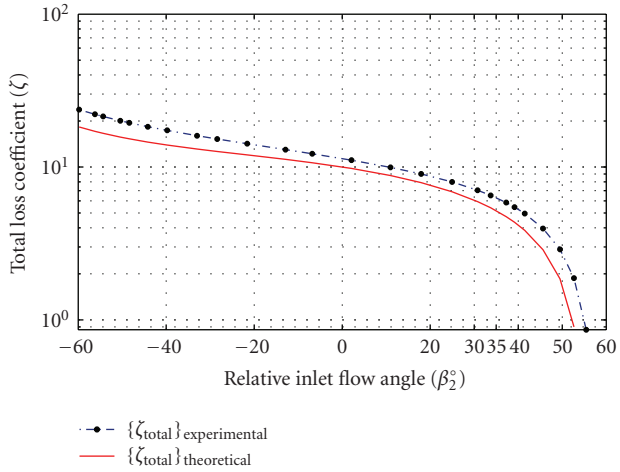

Figure 12: Turbine loss coefficient versus inlet flow angle (β_2) [10].

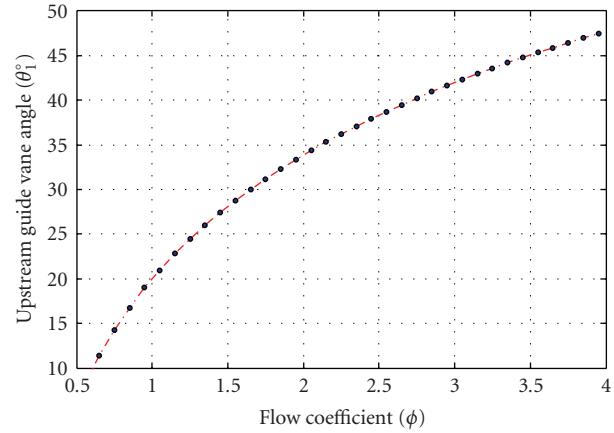

Figure 13: Upstream guide vane angle versus flow coefficient.

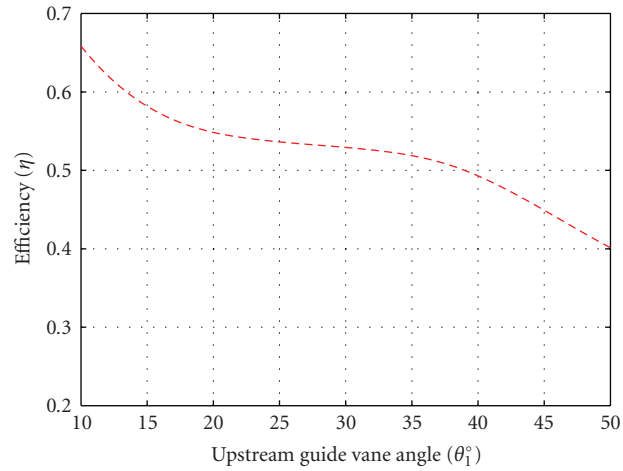

Figure 14: Efficiency versus upstream guide vane setting up angle.

increase of relative inlet flow angle following two different curvatures with an inflexion point that is located at $\beta_2 = 0^\circ$. The latter angle does not represent the minima point as seen from Figure 11. The minima scenario would be typical to a reaction turbine with an optimum angle not necessarily 0° [11]. Therefore, though the reported experimental pressure drop across the turbine rotor was substantial [4, 18], the loss reported in the present study reinforces the impulse characteristic of this particular turbine for which there is no negative or positive stall. In other word, there is no high positive or negative incidence for which the air flow separates catastrophically from the blade surface resulting in sudden collapse of torque and increase in pressure drop and therefore of loss.

In order to identify the optimum inlet flow angle for which the impulse turbine efficiency is maximum, a semilog graph was used.

As we can see from Figure 12, the total loss coefficient follows a straight portion with a moderate slope from low inlet angle up to around $\beta_2 = 35^\circ$ from which point the loss starts decreasing rapidly for the rest of the turbine operational range. As a result the optimum inlet flow angle, at which the turbine efficiency is maximum (the optimum performance of this particular turbine is reached at lower level of flow coefficient), was found to be $\beta_2 = 35^\circ$. The experimental value reported in [4] was $\beta_2 = 33.8^\circ$.

Figure 13 shows variation of the optimum upstream guide vane angle with the flow coefficient while keeping the relative inlet flow angle optimum $\beta_2 = 35^\circ$. For lower flow coefficient, the guide vane angle is small because of the lower input power, whereas at higher flow coefficient region, where the impulse turbine is known to handle larger input power without drastic decrease of efficiency (unlike the Wells turbine), the guide vane angle is larger. This is in order to satisfy the turbine optimum relative inlet angle.

Figure 14 shows the model prediction of the impulse turbine efficiency when the upstream guide vanes setting up angle is changed from 13° to 46° while keeping the relative inlet flow angle optimum $\beta_2 = 35^\circ$ (see Figure 12). As we can see the efficiency at each flow coefficient hence corresponding upstream guide vanes setting up angle is improved for the majority of flow coefficient especially at lower flow coefficient range.

6. CONCLUSIONS

An explicit new quasi-steady analytical model based on the well-known angular momentum principle and Euler turbine equation for predicting the impulse turbine performance was presented. The accuracy of the model has been verified using previously carried out experimental study. The predicted torque coefficient was found to fit well the experimental data. The input coefficient, which is directly related to the pressure drop across the turbine which in turn is greatly affected by the generated losses, is also well predicted up to high region of flow coefficient. Furthermore, the model predicted the turbine efficiency with a fair accuracy (2%) overall.

The evolution of the flow incidence and absolute exit angle on the rotor blade leading edge and trailing edge, respectively, with the flow coefficient has not been reported up till now in the literature of this type impulse turbine.

This gave a deep insight in understanding the behavior of impulse turbine wave energy extraction. Furthermore, it has been elucidated that the downstream guide vane plays an important role in the impulse turbine efficiency.

However, the proposed model for performance prediction could be further improved by incorporating tip clearance and viscous losses in order to predict the turbine total loss more accurately.

The usefulness of the presented model consists of its capability to quantify and provide a basis for comparing performance of the self-rectifying impulse turbines. This would allow the designer to size an impulse turbine to a given wave power application.

NOMENCLATURE

D:	Turbine diameter (m)
ν:	Hub-to-tip ratio
$D_R = (1+\nu)(D/2)$:	Turbine mean radius (m)
$r_R = D_R/2$:	Turbine rotor mean radius (m)
Z:	Number of turbine blades
$S_r = \pi D_R/Z$:	Blade pitch (m)
$L_r = 2S_r$:	Blade axial chord length (m)
$\text{sigma}_r = S_r/L_r$:	Turbine rotor solidity
T_a:	Width path flow in (m)
$b = (1-\nu)(D/2)$:	Blade height in (m)
V_a:	Air axial velocity (m/s)
U_R:	Blade linear velocity at midspan (m/s)
$\phi = V_a/U_R$:	Flow coefficient
θ_1:	Upstream guide vane angle
α_2:	Absolute inlet flow angle
V_2:	Absolute inlet flow velocity (m/s)
β_2:	Relative inlet flow angle
W_2:	Relative inlet flow velocity (m/s)
β_3:	Relative exit flow angle
W_3:	Relative exit flow velocity (m/s)
α_3:	Absolute exit flow angle
V_3:	Absolute exit flow velocity (m/s)
θ_2:	Downstream guide vane angle
$V_{\theta 2}$:	Absolute inlet flow tangential velocity
$V_{\theta 3}$:	Absolute exit flow tangential velocity
$\Delta V = V_{\theta 2} - (-V_{\theta 3})$:	Change of air whirl velocity (m/s)
γ:	Blade angle
$i = \beta_2 - \gamma$:	Incidence angle
$d = \beta_3 - \gamma$:	Deviation angle
$\epsilon = \beta_2 - \beta_3$:	Angle between the relative and absolute flow vector at inlet and outlet of the rotor
ρ:	Air density (Kg/m^3)
$Q = b\pi D_r V_a$:	Volumetric flow rate (m^3/s)
$\dot{m} = \rho Q$:	Air mass flow rate (Kg/s)
T_o:	Torque on shaft (N·m)
$\omega = U_R r_R$:	Turbine rotor rotational speed (rd/s)
$P_o = T_o \omega$:	Turbine rotor power output (watt)
$P_{02} - P_{03}$:	Total stagnation pressure across the rotor (Pa)
ΔP_{th}:	Theoretical pressure drop across the rotor (Pa)
ΔP_L:	Pressure losses through the turbine (Pa)
$\Delta P = \Delta P_{\text{th}} + \Delta P_L$:	Actual pressure gradient across the turbine (Pa)
I_{th}:	Theoretical enthalpy drop of the turbine
ΔI_1:	Enthalpy loss through the turbine
$\Delta I = \Delta I_{\text{th}} + \Delta I_1$:	Actual enthalpy drop through the turbine
ζ_R:	Rotor loss coefficient
ζ_{GV}:	Downstream guide vane loss coefficient
$\zeta = \zeta_R + \zeta_{\text{GV}}$:	Total loss coefficient.

REFERENCES

[1] A. F. de O. Falcão, "First-generation wave power plants: current status and R&D requirements," *Journal of Offshore Mechanics and Arctic Engineering*, vol. 126, no. 4, pp. 384–388, 2004.

[2] T. Setoguchi and M. Takao, "Current status of self rectifying air turbines for wave energy conversion," *Energy Conversion and Management*, vol. 47, no. 15-16, pp. 2382–2396, 2006.

[3] A. Thakker and F. Hourigan, "Modeling and scaling of the impulse turbine for wave power applications," *Renewable Energy*, vol. 29, no. 3, pp. 305–317, 2004.

[4] B. K. Hammad, *Design analysis of the impulse turbine with fixed guide vanes for wave energy power conversion*, Doctoral thesis, Department of Mechanical & Aeronautical Engineering, University of Limerick, Limerick, Ireland, 2002.

[5] J. D. Denton and L. Xu, "The exploitation of three-dimensional flow in turbomachinery design," *Proceedings of the Institution of Mechanical Engineers, Part C: Journal of Mechanical Engineering Science*, vol. 213, no. 2, pp. 125–137, 1999.

[6] J. I. Cofer, J. K. Reinher, and W. J. Summer, "Advances in steam path technology," in *Proceedings of the 39th GE Turbine State-of the-Art Technology Seminar*, vol. 125, August 1993, GER-3713D.

[7] T. C. Booth, "Importance of tip clearance flows in turbine design," in *Tip Clearance Effects in Axial Turbomachines*, Lecture Series, p. 134, von Karman Institute for Fluid Dynamics, Rhode Saint Genèse, Belgium, 1985.

[8] S.-Y. Cho and S.-K. Choi, "Experimental study of the incidence effect on rotating turbine blades," *Proceedings of the Institution of Mechanical Engineers, Part A: Journal of Power and Energy*, vol. 218, no. 8, pp. 669–676, 2004.

[9] A. Thakker, T. S. Dhanasekaran, and J. Ryan, "Experimental studies on effect of guide vane shape on performance of impulse turbine for wave energy conversion," *Renewable Energy*, vol. 30, no. 15, pp. 2203–2219, 2005.

[10] T. S. Dhanasekaran, *Computational and experimental analysis on flow and performance of impulse turbine for wave energy conversion*, Doctoral thesis, Department of Mechanical & Aeronautical Engineering, University of Limerick, Limerick, Ireland, 2004.

[11] R. I. Lewis, *Turbomachinery Performance Analysis*, Butterworth-Heinemann, Oxford, UK, 1st edition, 1996.

[12] P. G. Hill and C. R. Peterson, *Mechanics and Thermodynamics of Propulsion*, Addison-Wesley, Reading, Mass, USA, 2nd edition, 1992.

[13] M. Inioue, K. Kaneko, and T. Setoguchi, "One-dimensional analysis of impulse turbine with self-pitch-controlled guide vanes for wave power conversion," *International Journal of Rotating Machinery*, vol. 6, no. 2, pp. 151–157, 2000.

[14] N. Wei, *Significance of loss models in aerothermodynamic simulation for axial turbines*, Ph.D. thesis, Royal Institute of Technology, Stockholm, Sweden, 2000.
[15] J. H. Horlock, *Axial Flow Turbines*, Butterworth, London, UK, 1966.
[16] B. Lakshminarayana, *Fluid Dynamics and Heat Transfer of Turbomachinery*, John Wiley & Sons, New York, NY, USA, 1996.
[17] A. Thakker and T. S. Dhanasekaran, "Computed effect of guide vane shape on performance of impulse turbine for wave energy conversion," *International Journal of Energy Research*, vol. 29, no. 13, pp. 1245–1260, 2005.
[18] A. Thakker, F. Hourigan, T. Setoguchi, and M. Takao, "Computational fluid dynamics benchmark of an impulse turbine with fixed guide vanes," *Journal of Thermal Science*, vol. 13, no. 2, pp. 109–113, 2004.
[19] A. Thakker and T. S. Dhanasekaran, "Computed effects of tip clearance on performance of impulse turbine for wave energy conversion," *Renewable Energy*, vol. 29, no. 4, pp. 529–547, 2004.